

Study of light cluster population in dilute nuclear matter from heavy ion vaporization events

A. REBILLARD-SOULIÉ for the INDRA and FAZIA COLLABORATIONS

Normandie Université, ENSICAEN, UNICAEN, CNRS/IN2P3, LPC Caen - Caen, France

received 26 November 2024

Summary. — An analysis work on vaporization events selected from $^{36}\text{Ar}+^{58}\text{Ni}$ collisions at 74 MeV/nucleons has been done. In the particle velocity spectrum, we evaluated the pollution from other sources of emission than the quasi-projectile. In particular, the HIPSE event generator has been used to estimate the shape of the polluting distribution. Moreover, the contribution of secondary decays in measured multiplicities has been evaluated using two-body correlations, where the non-resonant background was evaluated with an event mixing technique.

1. – Introduction

Light clusters in low density nuclear matter play a significant role as they constitute an important part of the chemical composition [1]. In core-collapse supernovae, the abundancies of these clusters can modify the propagation of neutrinos and the shock-wave through the matter [2]. Several approaches describe the nuclear matter with light clusters like the relativistic mean-field model [3]. In this model, the coupling constant of the clusters with the medium needs to be calibrated using experimental observations like heavy-ion collisions.

In this contribution, we will present an analysis of experimental data from heavy-ion collisions detected with INDRA-FAZIA apparatus. We will show a method to select particles that can be attributed to a source at the projectile velocity (*i.e.*, the quasi-projectile or QP). We will also present an estimation of the particles coming from secondary decays using multi-particle correlation techniques. All the analysis is done for each of the studied isotopes (^1H , ^2H , ^3H , ^3He and ^4H) but in this contribution, we only present the ^4He .

2. – Experimental details

The 2nd INDRA-FAZIA experiment was conducted in April and May 2022. This is the first experiment since the full renewal of INDRA's electronics which is now digital [4]. Two beams were dedicated to physics: ^{36}Ar and ^{58}Ni (only the argon beam is used in

the present work). Both were at 74 MeV/nucleon of incident energy and impinging on a 410 μm thick ^{58}Ni target. INDRA is composed of 96 silicon (Si) detectors and 240 cesium iodide crystals (CsI) covering from 14° to 176° of the angular space [5]. FAZIA is composed of 192 Si-Si-CsI telescopes from 2° to 14° [6] corresponding to the forward removed part of INDRA. The isotopic identification is achieved through two techniques: ΔE - E and pulse-shape analysis depending on the energy and the mass of the detected particle. It can go up to $Z = 25$, which makes it sufficient to identify the products of the ^{36}Ar .

3. – Event selections

3.1. Vaporisation. – In nuclear matter, the vaporization stands for the transformation of the system for uniform, liquid-like matter to a gas of free nucleons with light clusters. In previously published works [7-9], events with only hydrogen and helium isotopes have been attributed to vaporization of the nuclear system. In our case, we want to study specifically the QP, whose decay products are located in the forward part of the center of mass (c.m.). Therefore, we consider only the particles whose parallel velocities are positive in the c.m. frame ($v_{z,cm} > 0$). Concretely, we impose the higher charge among all particles detected in the forward part of the c.m. to be 2 or less ($Z_{max}^{front} \leq 2$).

3.2. Completeness. – To ensure we detect the higher charge, we need a completeness criterion keeping only the events with most of the projectile's products detected. We impose the charge measured at the forward part of the c.m. to be greater than or equal to 16 ($Z^{front} \geq 16$).

3.3. Centrality. – To study the vaporization of the QP, we need to be sure such a source can be identified and if other sources exist, suppress their contributions. The centrality⁽¹⁾ of the collision is a good estimation of its violence and can be linked to global event observables like the total transverse kinetic energy of light particles of total multiplicity. In our case we choose the parallel velocity of the frame constructed from all particles at the forward part of the c.m., $V_{front} = \frac{\sum m_i \times v_i}{\sum m_i} |_{v_{z,cm} > 0}$, where v_i and m_i are the velocity and mass of the particles in the event. Figure 1(a) presents V_{front} as a function of the impact parameter b for events generated by HIPSE, a classical statistical event generator [10]. We observe that the lower (higher) values of V_{front} corresponds to the most central (peripheral) collisions with a monotonous relation. We can now define three centrality regions:

- I) $V_{front} < 3.5$ cm/ns: central collisions with $\langle b_{HIPSE} \rangle = 2.5$ fm.
- II) 3.5 cm/ns $< V_{front} < 4.5$ cm/ns: semi-peripheral collisions with $\langle b_{HIPSE} \rangle = 4$ fm.
- III) $V_{front} > 4.5$ cm/ns: peripheral collisions with $\langle b_{HIPSE} \rangle = 6.3$ fm.

Figure 1 presents the V_{front} distribution for the selected events with the different centrality regions.

For each centrality region, we look at the particle velocity distribution, as presented in fig. 2 for the ^4He . We observe that for the most central collisions, the ^4He are essentially

⁽¹⁾ The centrality can be defined as how close the centers of the colliding nuclei are to each other in the transverse plane with respect to the beam axis.

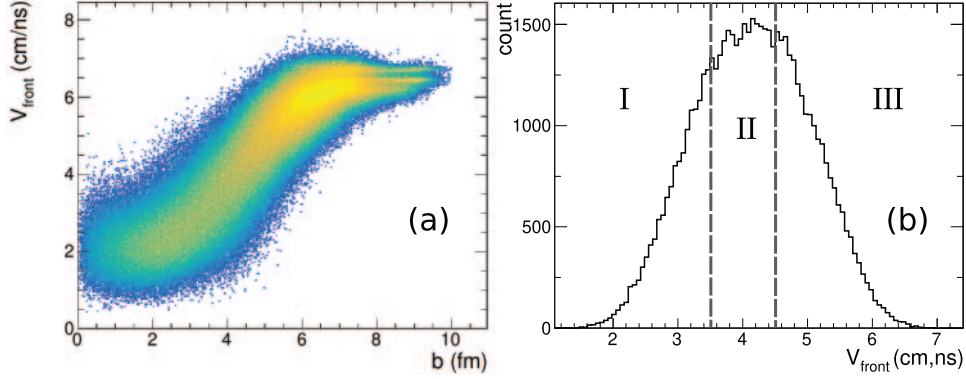


Fig. 1. – Correlation between V_{front} and impact parameter b for events generated with HIPSE (a). Distribution of V_{front} for complete QP vaporisation events with the three defined centrality regions (see text) (b).

located close to the c.m. velocity (around $V_Z = 4$ cm/ns), also called the mid-velocity region. These particles are emitted from a source that is not the QP, we call it hereafter the “non-QP” emission. As the collisions get more peripheral, the emitted ${}^4\text{He}$ move towards velocities close the one of the QP (around $V_Z = 11$ cm/ns) indicating an emission from the QP. For the present work, we select only the event corresponding to the peripheral region ($V_{front} > 4.5$ cm/ns) where most of the “non-QP” emission is suppressed. However, a minor “non-QP” contribution is still present and constitutes a pollution we want to get rid of.

4. – Projectile-like source selection

While the centrality selection suppresses most of the non-QP pollution, this later remains present and needs to be properly estimated. We propose to construct multiple ensembles in V_{front} as the proportion of non-QP emission evolves with this variable. The

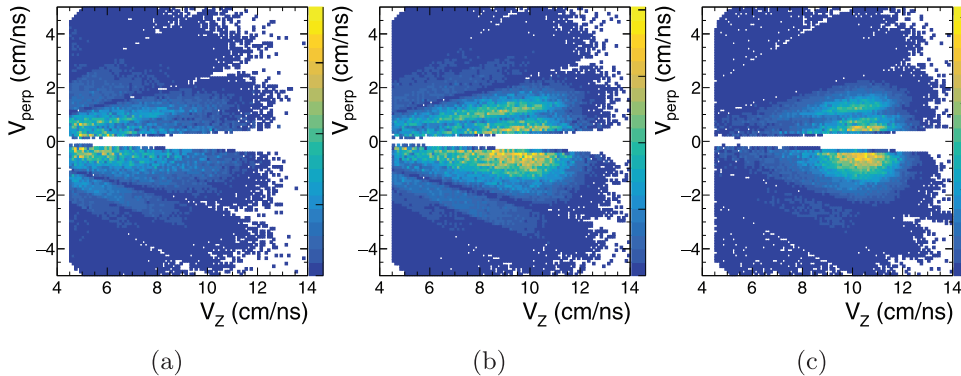


Fig. 2. – Parallel *vs.* perpendicular velocities (with respect to the beam axis) of the ${}^4\text{He}$ for each centrality region: central (a), semi-peripheral (b) and peripheral (c).

events are then classified into 7 different ensembles from $V_{front} = 4.5$ cm/ns to $V_{front} = 6.25$ cm/ns. In the following, we will present only three ensembles: 4.5–4.75 cm/ns, 5–5.25 cm/ns and 5.75–6 cm/ns.

We present a method to estimate the non-QP emission based on the HIPSE event generator where we have access to the origin of the particles. The parallel velocity distributions of ${}^4\text{He}$ from HIPSE events are presented in fig. 3 where the QP and non-QP contributions are distinguished. As already observed, the non-QP pollution is centrality dependent with more polluted spectrum for the most central collisions. This non-QP contribution presents a nearly linear behaviour, decreasing with the parallel velocity and maximum (in proportion) at the beginning of the total distribution and minimum at its end. We now approximate the contribution to an affine function with the two extremum construction points.

Figure 4 presents the same velocity distributions as in fig. 3 but for the experimental data where we do not have access to the origin of the particles. However, since the distributions appear to be similar to HIPSE's ones, we can construct an affine distribution in the same way, as presented with the black lines in fig. 4. The lines are doubled because of the uncertainty in the determination of the starting point. The proportion from these non-QP regions can be directly estimated by computing the ratio between the total and the non-QP integral. The non-QP proportion for the different considered species presents the same behaviour: the pollution decreases as the collisions gets more peripheral (or increasing V_{front}). In the experimental data, the pollution for ${}^4\text{He}$ is estimated around 35% for the first presented ensemble (4.5–4.75 cm/ns) and around 3% for the last presented ensemble (5.75–6 cm/ns). It is then important to carefully estimate this contribution for further analysis.

5. – Secondary decays estimation

When looking to the products from the deexcitation of the QP, we can expect secondary decays to occur. The products of these secondary decays cannot be treated as the products primarily generated in the collision. We need to estimate their contribution while we consider here only the following two-body reconstructions: ${}^1\text{H}+{}^4\text{He} \rightarrow {}^5\text{Li}$, ${}^2\text{H}+{}^4\text{He} \rightarrow {}^6\text{Li}$ and ${}^4\text{He}+{}^4\text{He} \rightarrow {}^8\text{Be}$, as they were evaluated to be the more dominant.

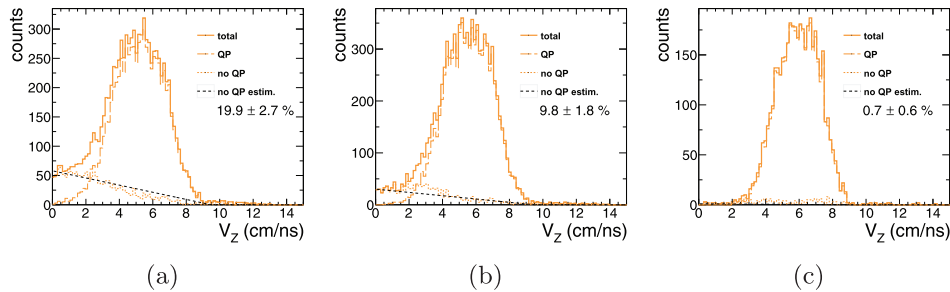


Fig. 3. – ${}^4\text{He}$ parallel velocity distributions in the c.m. from HIPSE for three ensembles: 4.5–4.75 cm/ns (a), 5–5.25 cm/ns (b), 5.75–6 cm/ns (c). Three contributions are printed: total (plain line), QP (dash line), non-QP (dotted line) and the proportion of non-QP particles is also printed.

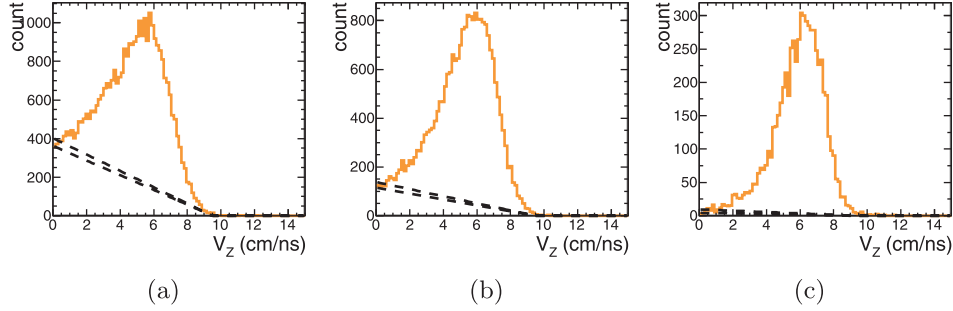


Fig. 4. – ${}^4\text{He}$ parallel velocity distributions in the c.m. from the selected events for three ensembles: 4.5–4.75 cm/ns (a), 5–5.25 cm/ns (b), 5.75–6 cm/ns (c). The black lines represent the non-QP distribution obtained by affine function fit.

5.1. Invariant mass reconstruction. – To see signals of these decays, we need to look at correlations between the collision products. When we have access to all reaction products, the invariant mass reconstruction is a commonly used technique that is based on the simple conservation of the relativistic mass of the system:

$$(1) \quad E^*(X) = E_{kin}(Y_1) + E_{kin}(Y_2) - Q_{X \rightarrow Y_1+Y_2},$$

where $E^*(X)$ is the excitation energy of the parent nucleus X and $E_{kin}(Y_{1,2})$ the kinetic energy of the daughter nuclei. Knowing the kinetic energy of the detected daughter nuclei, we are able to compute the excitation energy of the parent excited nucleus. For each event, we make all possible combinations of the products of the three decays of interest. Each combination gives an excitation energy but the nuclei are not necessarily correlated. As a consequence, we observe some resonances but an important non-resonant background is present and needs to be suppressed, as presented in fig. 5 (black line). The total excitation energy distribution can be expressed as follows:

$$(2) \quad Y_{total}(E^*) = Y_{reson.}(E^*) + Y_{non-reson.}(E^*).$$

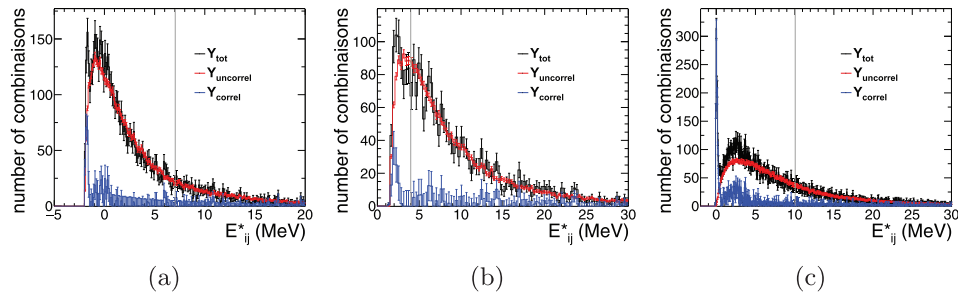


Fig. 5. – Excitation energy distributions for ${}^1\text{H}+{}^4\text{He} \rightarrow {}^5\text{Li}$ (a), ${}^2\text{H}+{}^4\text{He} \rightarrow {}^6\text{Li}$ (b) and ${}^4\text{He}+{}^4\text{He} \rightarrow {}^8\text{Be}$ (c) reconstructions. The event mixing background (red) and the background corrected spectrum (blue) are shown.

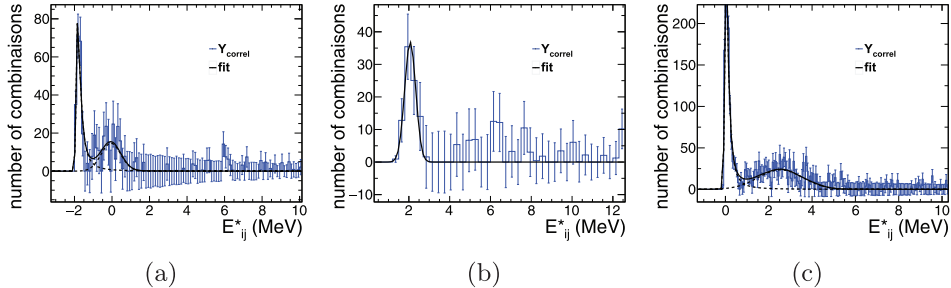


Fig. 6. – Corrected excitation energy distributions for ${}^1\text{H}+{}^4\text{He} \rightarrow {}^5\text{Li}$ (a), ${}^2\text{H} + {}^4\text{He} \rightarrow {}^6\text{Li}$ (b) and ${}^4\text{He}+{}^4\text{He} \rightarrow {}^8\text{Be}$ (c) reconstructions. The states fits (black) are shown.

5.2. Event mixing background. – The event mixing is a widely used technique to estimate the non-resonant background. The method consists in making combinations with nuclei taken from independent events which are in this way necessarily uncorrelated. We construct an excitation energy in the same way as for the single event reconstructions. One drawback of this method is that the accessible phase space differs from that of single event combinations. For instance, nuclei from independent events do not feel mutual Coulombian repulsion and can have lower relative momentum. This can be corrected by adding a Gamow Coulomb correction factor [11]. Figure 5 presents the excitation energy distributions for the three reconstructions of interest with the corrected background (in red) and the background corrected distribution (in blue).

5.3. Particle multiplicities. – Finally, we can extract the number of particles coming from secondary decays by integrating the number of counts in the corrected spectrum which are presented in fig. 6. Since the statistic is low and big fluctuations can be observed, we make fits of the different resonances that have been identified using Gaussian and Landau functions. For the ${}^5\text{Li}$ reconstructions two peaks are visible: the first around -2 MeV might corresponds to a sequential process with one missing product; the second one around 0 MeV corresponds to the ground-state. For the ${}^6\text{Li}$, one visible peak around 2 MeV corresponds to the first 3^+ state at 2.186 MeV . For the ${}^8\text{Be}$ reconstructions, two peaks are visible: one corresponding to the ground-state and the other to the first 2^+ state at 3.03 MeV . The proportions of particles coming from those decays are computed as the ratio between peak integrals and total multiplicity for a given species. The estimated proportions are: 2.7% for the ${}^1\text{H}$, 1.27% for the ${}^2\text{H}$ and 5.98% for the ${}^4\text{He}$.

6. – Conclusion

In this contribution, we presented an analysis of events attributed to the QP vaporization in ${}^{36}\text{Ar}+{}^{58}\text{Ni}$ collisions at 74 MeV/nucleon . We presented a method to estimate particle pollution from the mid-velocity emission for ${}^4\text{He}$ particles (other species are not shown but are also studied). In the presented results, the pollution increases with the centrality of the collision and is present in small proportions for the most peripheral ones. Within an invariant mass reconstruction, we analysed the two-body correlations and estimated the contribution of secondary decays. The non-resonant background has been estimated using an event-mixing technique. The contribution from these decays is estimated to be less important than the non-QP emission but still significant. These results indicate the need to carefully characterise the different contributions to the measured multiplicities when analysing emission from sources like the QP.

REFERENCES

- [1] TYPEL S. *et al.*, *Phys. Rev. C*, **81** (2010) 015803.
- [2] FISCHER T. *et al.*, *Phys. Rev. C*, **102** (2020) 055807.
- [3] PAIS H. *et al.*, *Phys. Rev. C*, **97** (2018) 045805.
- [4] FRANKLAND J. D. *et al.*, *Nuovo Cimento C*, **45** (2022) 43.
- [5] POUTHAS J. *et al.*, *Nucl. Instrum. Methods Phys. Res. A*, **357** (1995) 418.
- [6] THE FAZIA COLLABORATION, *Eur. Phys. J. A*, **50** (2014) 47.
- [7] BACRI CH. O. *et al.*, *Phys. Lett. B*, **353** (1995) 27.
- [8] BORDERIE B. *et al.*, *Phys. Lett. B*, **388** (1996) 224.
- [9] RIVET M. F. *et al.*, *Phys. Lett. B*, **388** (1996) 219.
- [10] LACROIX D. *et al.*, *Phys. Rev. C*, **69** (2004) 054604.
- [11] ZAJC W. A. *et al.*, *Phys. Rev. C*, **29** (1984) 2173.